The structural and biophysical basis of substrate binding to the hydrophobic groove in Ubiquilin Sti1 domains

Joan Onwunma[1]*, Saeed Binsabaan[2]*, Shawn P. Allen[1,2], Banumathi Sankaran[3], and Matthew L. Wohlever[1,2]

[1]Previously at University of Toledo, Department of Chemistry & Biochemistry
[2]University of Pittsburgh, Department of Cell Biology
[3]Lawrence Berkley National Lab, Berkeley Center for Structural Biology, Molecular Biophysics and Integrated Bioimaging
*These two authors contributed equally

Abstract
Ubiquilins are a family of cytosolic proteins that ferry ubiquitinated substrates to the proteasome for degradation. Recent work has demonstrated that Ubiquilins can also act as molecular chaperones, utilizing internal Sti1 domains to directly bind to hydrophobic sequences. Ubiquilins are associated with several neurodegenerative diseases with point mutations in UBQLN2 causing dominant, X-linked Amyotrophic Lateral Sclerosis (ALS). The molecular basis of Ubiquilin chaperone activity and how ALS mutations in the Sti1 domains affect Ubiquilin activity are poorly understood. This study presents the first crystal structure of the Sti1 domain from a fungal Ubiquilin homolog bound to a transmembrane domain (TMD). The structure reveals that two Sti1 domains form a head-to-head dimer, creating a hydrophobic cavity that accommodates two TMDs. Mapping the UBQLN2 sequence onto the structure shows that several ALS mutations are predicted to disrupt the hydrophobic groove. Using a newly developed competitive binding assay, we show that Ubiquilins preferentially bind to hydrophobic substrates with low helical propensity, motifs that are enriched in both substrates and in Ubiquilins. This study provides insights into the molecular and structural basis for Ubiquilin substrate binding, with broad implications for the role of the Sti1 domain in phase separation and ALS.

Introduction
Defects in protein homeostasis (proteostasis) are key drivers of neurodegenerative diseases [1]. Ubiquilins are a family of proteins at the nexus of the cellular proteostasis network with links to the ubiquitin proteasome system, autophagy, and biomolecular condensates[2–8]. Ubiquilins have also been linked to numerous neurodegenerative diseases, with point mutations in UBQLN2 causing dominant, X-linked Amyotrophic Lateral Sclerosis (ALS)[8–12]. Humans have three widely expressed Ubiquilin paralogs, UBQLN1, UBLQN2, and UBLQN4, which are characterized by an N-terminal Ubiquitin Like (UBL) domain, two Sti1 domains, and a C-terminal Ubiquitin Associated (UBA) domain, separated by long stretches of intrinsically disordered regions (IDRs) [13] **(Figure 1A)**. UBQLN2 also contains a unique PXX region, which is a hotspot for many ALS mutations. Consequently, mutations in the PXX region have garnered intense interest. However, recent studies have identified additional ALS mutations in the UBQLN2 Sti1 domains which remain poorly characterized[14].

Most previous studies have focused on the role of Ubiquilins as proteasomal shuttle factors which facilitate client protein degradation[15–18]. Ubiquilins also have intrinsic chaperone activity, which is comparatively understudied[19,20]. Previous work has shown that Ubiquilin Sti1 domains can directly bind to moderately hydrophobic transmembrane domains (TMDs) a motif that is particularly enriched among mitochondrial membrane proteins[21,22]. While the Sti1 domains are rich in methionine residues, a hallmark of many TMD binding proteins[23–25], the molecular basis for selectively binding moderately hydrophobic TMDs is unclear. Sti1 domains are a common motif in proteostasis and can be broadly categorized into co-chaperone and adaptors of the

Ubiquitin Proteasome System[26,27]. There is little structural data on the proteasome adaptor family Sti1 domains, which includes Ubiquilins. While several modeling studies, including AlphaFold, have predicted the rough shape of the Ubiquilin Sti1 domain[26,28], these predictions have low confidence. The lack of experimental structural data on Sti1 domain chaperone activity is thus a major roadblock in the field.

Another hallmark of Ubiquilins is the ability to phase separate and form biomolecular condensate[29,30]. While the physiological role of Ubiquilin phase separation is still being elucidated, many ALS mutants display altered phase separation properties[8,14,31]. Interestingly, the Sti1-II domain is essential for UBQLN2 condensate formation, but how this domain contributes to phase separation is unclear[29].

Here, we present a crystal structure of a Sti1 domain from a fungal Ubiquilin homolog bound to a TMD. Two Sti1 domains form a head-to-head dimer to generate a hydrophobic cavity that can accommodate two TMDs. Mapping the UBQLN2 sequence on the structure shows that several ALS mutations are predicted to disrupt this hydrophobic groove. We also developed a competitive binding assay to determine the biophysical properties that govern substrate binding to the Sti1 domains. Using this assay, we determined that Ubiquilins preferentially bind to hydrophobic regions with low helical propensity. These biophysical properties are enriched in known Ubiquilin substrates and within the Ubiquilin IDRs. We propose that internal IDRs serve as placeholders in the Sti1 hydrophobic groove that are displaced upon encounter with a bona fide substrate. Together, our data presents the first crystal structure of a Ubiquilin Sti1 domain, rationalizes several ALS mutations, and provides a model for how the Sti1 domain drives Ubiquilin phase separation.

Results

Crystal structure of the Sti1 domain bound to a TMD

Ubiquilin Sti1 domains are flexible and have short-lived interactions with substrates, making them challenging targets for traditional structural biology approaches[21,26]. To stabilize the Sti1-TMD interaction we generated a fusion construct consisting of the Sti1 domain from *M. bicuspidata* Dsk2, a variant of the VAMP2 TMD, and the receiver domain from *Myxococcus xanthus* social motility protein FrzS as a crystallization scaffold[32]. FrzS was chosen because it robustly crystallizes at high resolution and has the N and C-termini positioned to allow for optimal interaction between the TMD and Sti1 domain[33]. The resulting construct formed crystals within three days at 4° C. We solved the crystal structure via molecular replacement with the FrzS domain with an overall resolution of 1.98 Å.

Our structure shows a domain swapped dimer, with the TMD of subunit 1 bind to the Sti1 domain of subunit 2 **(figure S1A)**. Two Sti1 domains stack head-to-head to create a fully enclosed hydrophobic cavity capable of chaperoning two TMDs **(Figure 1 & S1)**. The presence of multiple TMDs within the hydrophobic groove is reminiscent of the crystal structure of the TMD chaperone and targeting factor GET3[34]. The dimerization of the Sti1 domain is thermodynamically appealing as it ensures that no part of the hydrophobic TMD is solvent exposed. Interestingly, the Sti1-II domain is essential for UBQLN2 dimerization, suggesting that dimerization of the Sti1 domain may be a key feature of the Ubiquilin/Dsk2 function[1,35,36]. The dimer is unlikely to be an artifact of crystallization as the two FrzS domains do not contact each other in the asymmetric unit and the crystallization construct runs as an oligomer on size exclusion chromatography **(Figure S1)**.

Each monomer is composed of 6 α-helices that assemble into a helical-hand or U-shape. Each of the sides of the helical-hand contain two α-helices connected by short loops with ~90° turns **(Figure 1D)**. The hydrophobic groove is enriched in methionine residues **(Figure S1D)**, a common feature of many membrane protein chaperones[23,37]. The overall shape is roughly similar to the AlphaFold prediction, however there are numerous differences in the details of TMD packing with the hydrophobic groove, highlighting the importance of experimental structural biology approaches **(Figure S1E)**. The TMD binds the bottom of the hydrophobic groove and buries ~2970 Å^2 of hydrophobic surface area with each Sti1 monomer. Key residues in the hydrophobic groove that contact the TMD include L190, M193, A207, M210, L211, M214, M218, M225, M228, and M229, which correspond to residues 30, 33, 47, 50, 51, 54, 58, 65, 68, and 69 in the crystallization construct. We conclude that the Sti1 domain forms a hydrophobic groove capable of forming head-to-head dimers that can fully encapsulate two TMDs.

Table 1. Data collection and refinement statistics

	Sti1-Frzs-TMD
Data collection	
Space group	P 1 21 1
Cell dimensions	
a, *b*, *c* (Å)	67.41 63.92 67.43
α, β, γ (°)	90.0, 98.83, 90.0
Resolution (Å)	66.63-1.98 (2.09-1.98)
Unique reflections	36912 (4887)
$\langle I / \sigma I \rangle$	17.7 (2.1)
R_{merge} [a]	0.056 (0.827)
R_{pim}	0.024 (0.367)
Completeness (%)	93.3 (85.9)
Redundancy	6.4 (6.0)
Refinement	
Resolution (Å)	46.127-1.98 (2.03-1.98)
R_{work} [b] / R_{free} [c] (%)	22.00- 23.21
No. atoms	3516
Protein (non-H)	3392
Water	124
Avg B-factors (Å^2)	55.45
Protein	55.67
Water	49.65
R.m.s. deviations	
Bond lengths (Å)	0.005
Bond angles (°)	0.80
Ramachandran	
Favored, Allowed, Outliers	99.09, 0.91, 0.0
Clashscore	6

Values in parentheses represent the outer resolution shell.
[a] $R_{merge} = (|(\Sigma I - \langle I \rangle)|)/ (\Sigma I)$, where $\langle I \rangle$ is the average intensity of multiple measurements.
[b] $R_{work} = \Sigma_{hkl}||F_o(hkl)|| - F_c (hkl)||/\Sigma_{hkl} |F_o(hkl)|$.

[c] R_{free} represents the cross-validation R factor for 5% of the reflections against which the model was not refined.

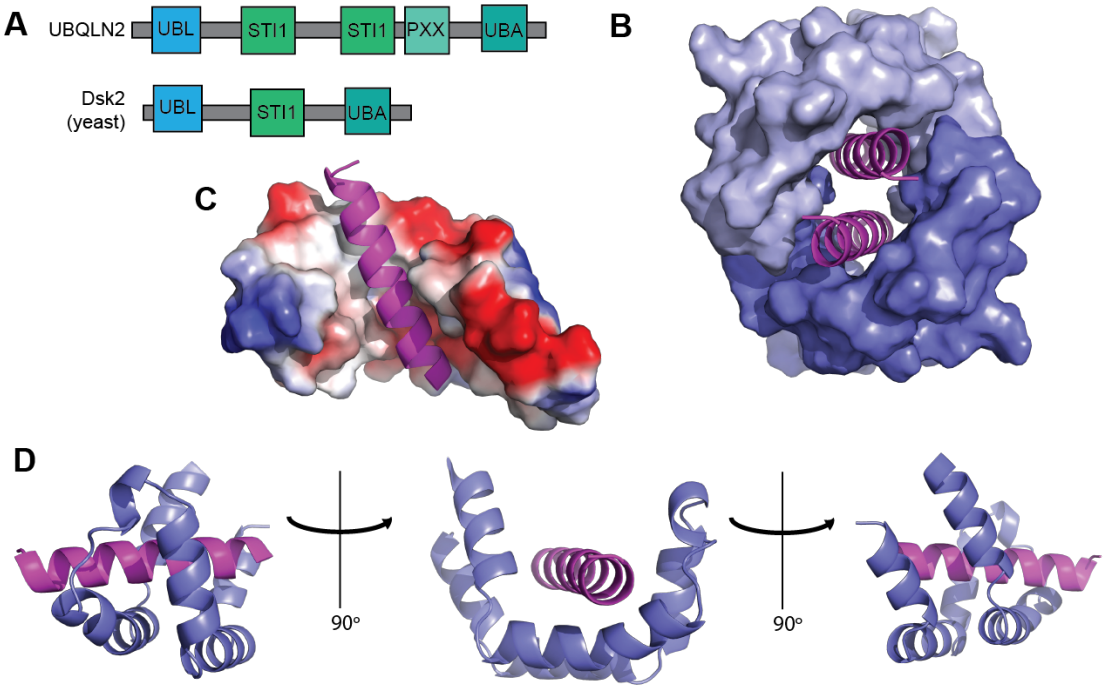

Figure 1: Crystal structure of the Dsk2 Sti1 domain bound to a TMD

A) Domain diagram of UBQLN2 and Dsk2.
B) Dimerization of the Dsk2 Sti1 domains forms a hydrophobic cavity that fully encapsulates two TMDs. Individual subunits are shown as a surface and TMDs are shown as cartoons (PDB: 9CKX).
C) Surface representation of Sti1 domain, colored by electrostatics. Note how the TMD binds in a hydrophobic groove.
D) Cartoon representation of a single Sti1 domain rotated around the y-axis.

<u>Several ALS Mutations are predicted to disrupt the Sti1 hydrophobic groove</u>

To gain a better understanding of how ALS mutations in the Sti1 domain affect Ubiquilin function, we performed a sequence alignment of the *M. bicuspidata* Sti1 domain against the Sti1-I or Sti1-II domains from UBLQN1, 2, and 4 **(Figure S2)**. The resulting sequence alignment was then mapped onto our crystal structure and the position of UBQLN2 ALS mutations was analyzed. Our structure predicts that the Q425R and M446R mutations will disrupt the hydrophobic groove via insertion of a charged residue **(Figure 2A & B)**. Notably, the AlphaFold prediction of UBQLN2 yields similar results.

The P189T and P440L mutations also occur in the UBQLN2 Sti1 domain but are not predicted to contact the TMD **(Figure 2C)**. Our analysis shows that the P189T and P440L mutations occur in short loops with a ~90° turn between sides of the helical-hand. The prolines and preceding residues have Phi-Psi angles that are uniquely favored by proline[38]. We propose that mutation of these highly conserved proline residues will disrupt folding of the Sti1 domain. We conclude that multiple UBQLN2 ALS mutations are predicted to disrupt the Sti1 hydrophobic groove.

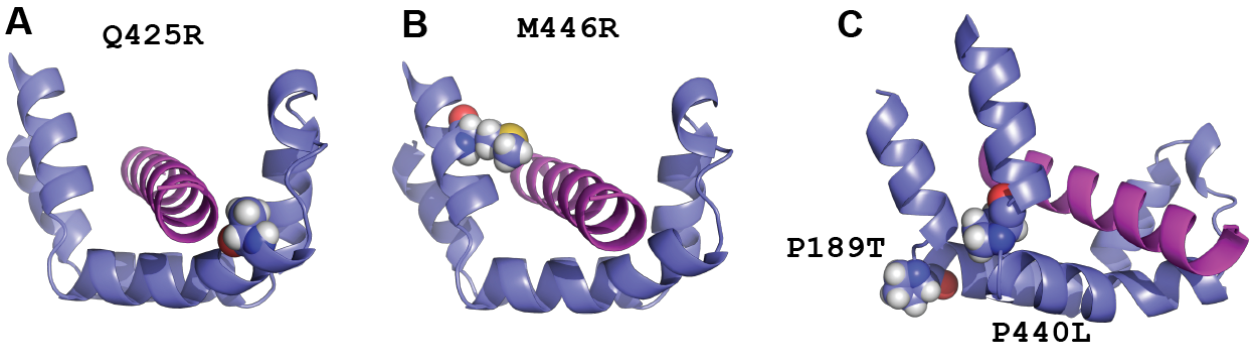

Figure 2: Several UBQLN2 ALS mutations are predicted to disrupt the Sti1 hydrophobic groove

A) The UBQLN2 sequence was mapped onto the Dsk2 structure. The UBQLN2 Q425R mutation, which causes ALS, is predicted to insert a charged residue into the Sti1 hydrophobic groove.
B) The UBLQN2 M446R mutation is also predicted to insert a charged residue into the Sti1 hydrophobic groove.
C) Residues P189 and P440 (spheres) in UBQLN2 are essential for forming the ~90° turns between α-helices in the helical hand motif. Mutation of these highly conserved residues is predicted to disrupt formation of the hydrophobic groove.

Development of a barcoded binding assay to study substrate binding to the Sti1 domain

It had been previously proposed that Ubiquilins selectively bind to moderately hydrophobic TMDs[21]. Our crystal structure shows a highly hydrophobic groove and cannot easily explain a preference for binding moderately hydrophobic TMDs. We therefore decided to rigorously test this model by developing a competitive binding assay.

We utilized the PURExpress In Vitro Transcription/Translation (IVT) system to produce ^{35}S labeled substrates in a detergent free environment[39]. The PURExpress reaction was supplemented with physiological concentrations of recombinantly purified flag-tagged Ubiquilin. To better mimic the complexity of the cellular environment, we sought to simultaneously present Ubiquilins with multiple closely related substrates. We developed a pool of six model substrates based on the TMD of Omp25, a mitochondrial tail anchored (TA) protein and known Ubiquilin substrate[21,40]. The hydrophobicity of the substrate TMDs, as assessed by Grand Average of Hydrophobicity (GRAVY) scores[41], was systematically varied by mutating residues to Alanine or Leucine. To differentiate substrates by SDS PAGE, a variable number of SH3 domains were added to serve as a "barcode" **(Figure 3A)**. The SH3 domain was chosen because it is small, well-folded, and contains no methionine residues which would bias the ^{35}S signal intensity[42]. After testing the expression of each plasmid individually, the six plasmids for a substrate series were mixed together such that expression of each model substrate was roughly equal. Ubiquilin-substrate complexes were purified by anti-Flag IP and binding was calculated by comparing the amount of substrate in the elution and input fractions.

Control experiments show that binding is dependent on the Sti1-TMD interaction. Deletion of the TMD shows interaction that is equivalent to our no Ubiquilin control, arguing that there is no interaction between Ubiquilins and the SH3 domains **(Figure 3B)**. Similarly, the previously characterized RRR TMD mutant[21], which has three Arginine mutations in the middle of the TMD,

disrupts substrate binding **(Figure 3C)**. Finally, we used our crystal structure and AlphaFold model to generate the UBLQN1 binding mutant, which contains two mutations in each Sti1 domain that are predicted to disrupt substrate binding. We observed no binding of any of the Omp25 substrates to the binding mutant, confirming that binding is dependent on the Sti1-TMD interaction **(Figure 3D)**.

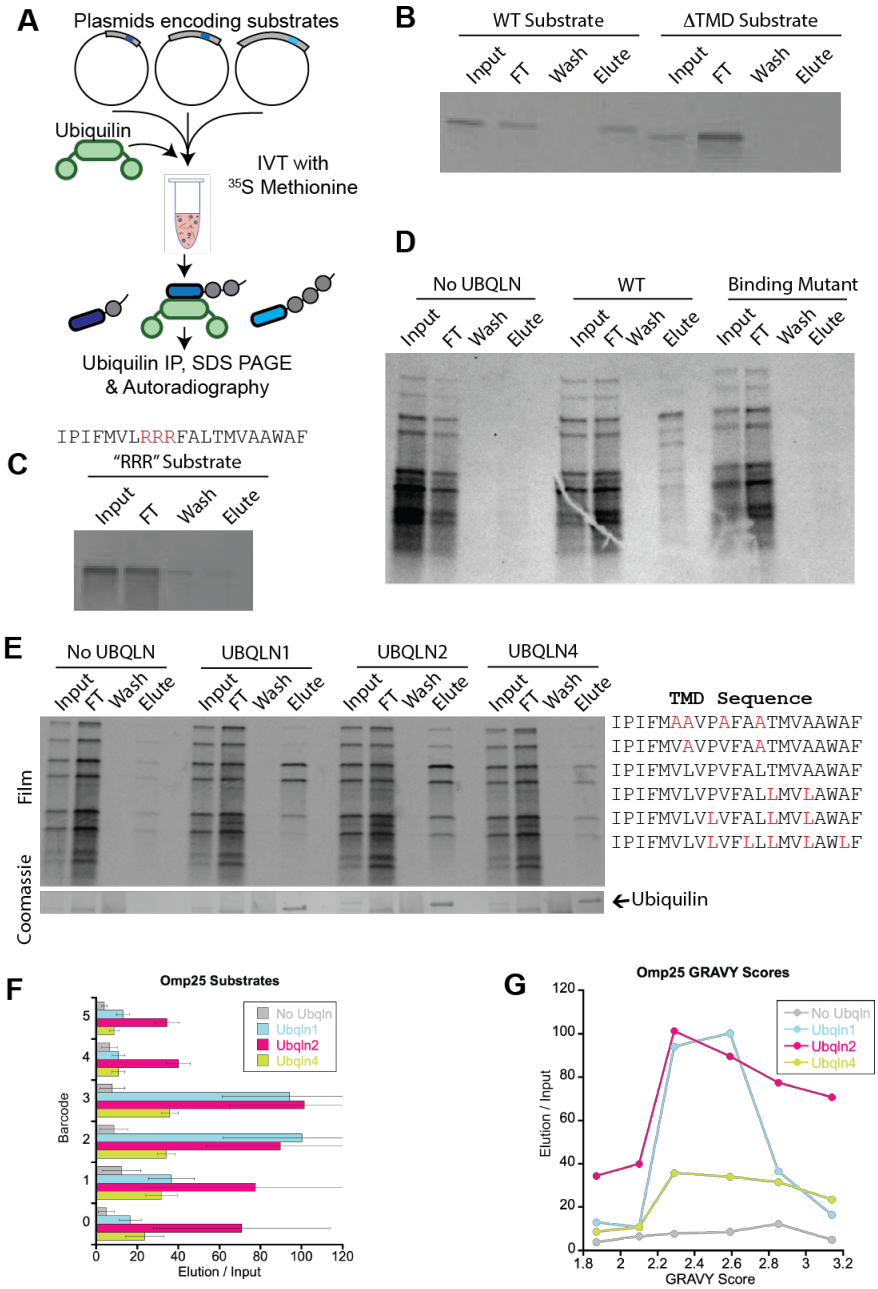

Figure 3: Development of barcoded binding assay to study Ubiquilin-substrate binding

A) Overview of the barcoded binding assay.
B) There is no biding to the barcode 3 construct when the TMD is deleted.
C) Mutation of the Omp25 TMD with three consecutive Arginine residues is sufficient to disrupt binding to Ubiquilin.
D) Substrate binding depends on interaction with the Sti1 domains. Binding assay with the Omp25 substrate series with no Ubiquilin control, WT UBQLN1, and the UBQLN1

binding mutant. The binding mutant contains two mutations in each Sti1 domain that are predicted to disrupt the hydrophobic groove (M186D, M228D, M394D, M454D).

E) Barcoded binding assay with the Omp25 substrate series. The wild type Omp25 TMD has a barcode of 3. Residues were mutated to either Leucine or Alanine to change TMD hydrophobicity.
F) Quantification of E, organized by barcode. Error bars are SEM. A value of 100 corresponds to equal intensity of input and elution bands.
G) Quantification of E, organized by TMD hydrophobicity (GRAVY). Error bars are omitted for clarity.

Ubiquilin paralogs show substantial overlap in substrate binding specificity

To test the substrate binding preference of Ubiquilins, we constructed a total of four substrate series, two based on the mitochondrial tail-anchored proteins Omp25 **(Figure 3E-G)** and Tom5 **(Figure S4)** and two based on the ER tail-anchored proteins Sec61β **(Figure S3)** and Vamp2 **(Figures S5)**. We chose tail-anchored proteins as our model substrates because they are verified Ubiquilin substrates and the single TMD simplifies data analysis. The wild type TMD sequence was placed in the middle of the series with a barcode of either 2 or 3 and the hydrophobicity of the TMD within a substrate series was varied by mutating residues to Leucine or Alanine such that the GRAVY score shifted by 0.2-0.3 for each substrate. The wild type sequences of the four series have a broad range of hydrophobicity values, with GRAVY scores ranging from 1.61 to 3.29.

The Omp25 and Sec61β substrate series showed that Ubiquilins bound preferentially to TMDs with moderate hydrophobicity **(Figure 3 & S3)**. This trend was conserved between UBQLN1, 2, & 4. However, the TMD hydrophobicity that elicited maximum Ubiquilin binding differed between the two substrate series. The Tom5 substrate series was the least hydrophobic substrate series **(Figure S4)**. It had the lowest overall level of binding. It still showed a preference for moderately hydrophobic TMDs, but the trend was much less pronounced than with Omp25 and Sec61β. The Vamp2 substrate series was the most hydrophobic series and, unexpectedly, showed the highest overall level of substrate binding with no clear up and down pattern **(Figure S5)**. Overall, our results show that UBQLN1, 2, & 4 show a general trend for binding to TMDs with moderate hydrophobicity. However, the TMD GRAVY score that elicited maximum substrate binding varied based on the substrate series. This suggests that TMD GRAVY score alone fails to fully capture the biophysical parameters that govern substrate binding.

We observed modest, but reproducible differences in the substrate binding preferences of the Ubiquilin paralogs. UBQLN4 consistently had the lowest levels of substrate binding, with the results being most pronounced in the Omp25 **(Figure 3)** and Tom5 **(Figure S4)** substrate series. Within the Vamp2 substrate series, which was the most hydrophobic series, there were no statistically significant differences in substrate binding **(Figure S5)**.

UBQLN1 and UBQLN2 showed roughly equal levels of substrate binding, with the exception of the least hydrophobic substrate series, Tom5. However, as TMD hydrophobicity reached the more extreme values, UBQLN1 binding dropped close to background levels whereas UBQLN2 binding remained significantly above background levels. This trend is clearest in the Omp25 substrate series **(Figure 3)**, but is also observed with Sec61β **(Figure S3)** and Tom5 **(Figure S4)**. Overall, we conclude that there are significant redundancies within the substrate binding preferences of UBQLN1, 2, & 4, but UBQLN2 has the most robust substrate binding and the broadest substrate range whereas UBQLN4 shows the lowest levels of substrate binding.

Ubiquilin Sti1 domains selectively bind hydrophobic substrates with low helical propensity

Although Ubiquilin binding within each substrate series showed maximal binding to TMDs with moderate hydrophobicity, the GRAVY score that elicited maximal binding differed between each substrate series. When all four substrate series are analyzed together, there is no discernable preference for moderately hydrophobic TMDs **(Figure 4A)**. This indicates that substrate GRAVY score alone is a poor predictor of Ubiquilin binding.

Previous studies had demonstrated that ER TA proteins have higher TMD hydrophobicity and higher helical propensity than mitochondrial TA proteins[22]. As Ubiquilins were shown to preferentially bind to mitochondrial membrane proteins[5,21], we asked if helical propensity also governed Ubiquilin substrate binding. The helical propensity of each TMD was calculated using the Agadir score[43–45], with a high Agadir score corresponding to a high helical propensity. There was no obvious correlation between Agadir score and Ubiquilin binding **(Figure 4B)**.

We next asked if a combination of TMD GRAVY and Agadir scores are a better predictor of Ubiquilin binding. When plotted together, we observed a striking anti-correlation between substrate binding and Agadir score **(Figure 4C)**. When plotted as a bubble chart, we observed that optimal Ubiquilin substrates are hydrophobic TMDs with a low helical propensity **(Figure 4D)**. As many hydrophobic residues also have high helical propensity, this could account for the previous observation that Ubiquilins preferentially bind to moderately hydrophobic TMDs. We conclude that Ubiquilins have no inherent defect in binding to highly hydrophobic TMDs and substrate binding requires a combination of sufficient hydrophobicity and low helical propensity.

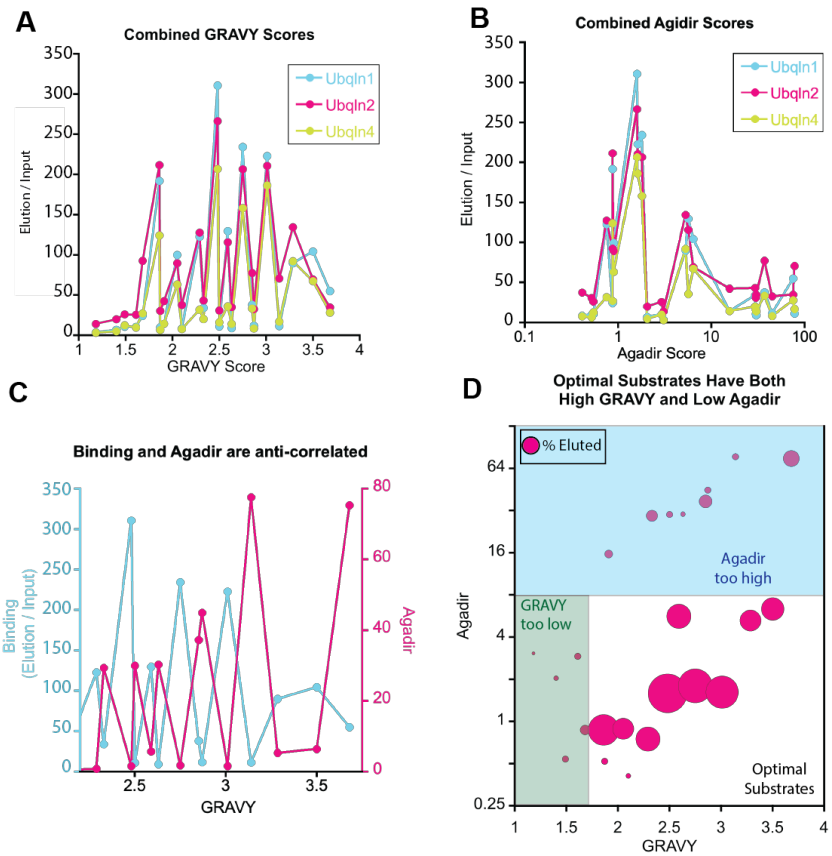

Figure 4: Barcoded binding assay shows that Ubiquilins bind to hydrophobic, disordered regions

A) Combined data from all four substrate series does not show a clear pattern between TMD GRAVY score and Ubiquilin binding.
B) Combined data from all four substrate series does not show a clear pattern between TMD Agadir score and Ubiquilin binding.
C) Combined data from all four substrate series shows that there is a strong anti-correlation between binding and Agadir scores.
D) Bubble chart shows that optimal Ubiquilin substrates have both a high GRAVY score and a low Agadir score.

Discussion

Here we present the crystal structure of the Sti1 domain of a fungal Ubiquilin homolog bound to a TMD. Our structure shows that two Sti1 domains form a head-to-head dimer that encapsulates two TMDs within a hydrophobic cavity. Each Sti1 domain forms a methionine rich hydrophobic groove, a common motif in TMD chaperones. Mapping the UBQLN2 Sti1 domains onto our crystal structure shows that several ALS mutations disrupt the hydrophobic groove. Dimerization is likely physiological as the Sti1-II domain is essential for UBQLN2 dimer formation and there are no obvious crystal contacts or interactions with the FrzS scaffold that can explain dimerization. More work is needed to understand the unique role of each Sti1 domain, the physiological consequences of disrupting substrate binding to the Sti1 domains, and the role of Sti1 dimerization in Ubiquilin function.

We also present a novel assay that measures TMD binding to Ubiquilin Sti1 domains in a complex, competitive environment. Using this assay, we discovered that Ubiquilin Sti1 domains preferentially bind to hydrophobic sequences with a low helical propensity, motifs which are enriched in both known Ubiquilin substrates and Ubiquilins themselves[2,36]. This raises provocative questions about the role of the Sti1 domains in Ubiquilin phase separation and how this activity can be dysregulated in ALS.

Ubiquilins were originally thought to preferentially bind moderately hydrophobic TMDs, so the observation that substrate selectivity is governed by both hydrophobicity and low helical propensity is unexpected. Previous binding assays lacked the precision to distinguish between these related, but distinct characteristics, likely accounting for the different descriptions of optimal Ubiquilin substrates. Interestingly, one of the distinguishing features of mitochondrial tail anchored proteins is low helical propensity of the TMD, which may account for the preferential binding of Ubiquilins to mitochondrial membrane proteins[5,46].

The structural features within the Sti1 domain that give rise to this substrate selectivity are unclear. It is tempting to speculate that the substrate TMD undergoes a disorder to helix transition upon binding to the Sti1 domain. Consistent with this proposal, the TMD in our fusion construct is predicted to have low helical propensity with an Agadir score of 1.59, but clearly forms a well-ordered helix in our crystal structure. Low helical propensity regions are important for several phase-separating systems, including RNA-binding protein TDP-43, the transcription factor Efg1, and Ubiquilins [29,47,48]. A low helical propensity region called the UBA-adjacent (UBAA) motif is present in both UBQLN1 and UBQLN2. Furthermore, this motif, together with the Sti1-II domain in UBQLN2, are critical for mediating phase separation[29,49,50]. We suspect that previous attempts to solve the crystal structure of the Sti1 domain were hampered by its intrinsic flexibility and that TMD binding may stabilize the Sti1 domain, allowing for crystal formation [26]. While not conclusive, our data is consistent with the substrate and/or Sti1 domain undergoing a

disorder to order transition upon binding, which may account for the preferential binding to TMDs with low helical propensity.

In the absence of a bound TMD, the methionine-rich hydrophobic groove within each Sti1 domain will have thermodynamically unfavorable interactions with solvent. Many TMD chaperones therefore use internal placeholder sequences to occupy the binding sites and act as a substrate selectivity filter that is displaced upon encounter with a bona fide substrate[34,46,51]. An analysis of the Dsk2 and UBQLN2 AlphaFold-predicted structures highlight several putative helical regions that may serve as placeholder sequences **(Figure S6)**. Indeed, paramagnetic spin labeling studies have shown that the UBQLN2 UBAA motif interacts with the Sti1-II domain[52].

We speculate that internal placeholders occupy the hydrophobic groove of Sti1 until a bona fide substrate is encountered **(Figure 5)**. Trans-interaction of the placeholder helix with the Sti1 domain of an adjacent Ubiquilin, much like we see in our domain swapped crystal structure, could contribute to the multivalency needed to drive phase separation. Indeed, size exclusion chromatography shows that the crystallization construct runs as an oligomer **(Figure S1)**. This could also explain the critical role of the Sti1 domain in Ubiquilin dimerization and phase separation. This model makes numerous predictions about the role of the Sti1 domain and proposed placeholders in substrate binding and Ubiquilin phase separation. Rigorously testing these predictions is a high priority.

Overall, our structural and biochemical analysis demonstrates the importance of Sti1 domains in Ubiquilin function and rationalizes how ALS mutations disrupt the Sti1 hydrophobic groove. We propose a model for how interaction of the Sti1 domain with internal placeholder sequences governs substrate selectivity and phase separation. This model presents a new paradigm for understanding Ubiquilin function and opens new avenues for therapeutic modulation of Ubiquilin substrate binding and phase separation to treat patients with ALS.

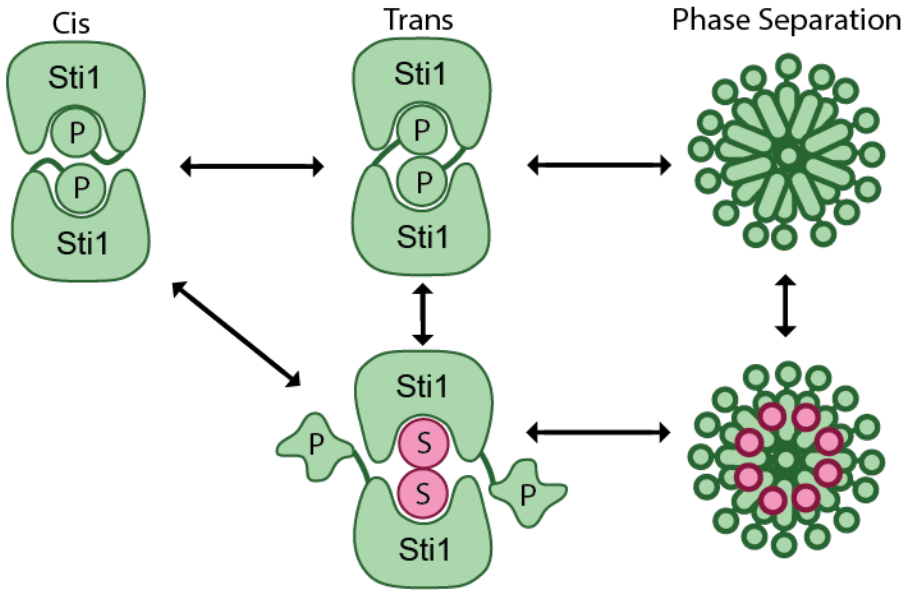

Figure 5: Proposed model for placeholder interaction with the Sti1 domain
In the absence of substrate, the placeholder sequence (P) occupies the Sti1 hydrophobic groove. This interaction can occur in Cis or Trans, with the Trans interaction providing the

multivalency that promotes Ubiquilin phase separation. Encounter with a true substrate (S), leads to the removal of the placeholder sequence with a potential loss of secondary structure.

Materials and Methods

Plasmid Construction

The bar-coded substrates have the general structure of 3xHA-Sec61β soluble domain, n x SH3, TMD, 3F4, where n varies between 0 and 5 to generate the barcode. The Omp25 substrates were generated by gene synthesis (Azenta) and cloned into the PURExpress DHFR Control Vector (NEB) between the NdeI and NotI sites. Note that each SH3 domain had a unique DNA sequence and unique restriction enzyme sites between the SH3 domains and the TMD. Subsequent substrate series were generated by replacing the TMD sequence with a new TMD sequence generated by gene synthesis. New TMD sequences were restriction cloned between KpnI and BamHI. Ubiquilin variants were cloned into pET28a vector and have the general structure of His_6-3C-3xFlag-Ubiquilin.

The crystallization construct was cloned into a pET28a vector with N-terminal His_6 tag followed by a 3C protease site. The fusion construct consisted of the Sti1 domain of M. bicupsidata Dsk2 (residues 165-234) followed by the receiver domain of *M. xanthus* FrzS (residues 3-124) and a variant of the Vamp2 TMD (MMIALGVACAIALAIAAVYF). The Vamp2 TMD is the same sequence used in the barcode 5 data which showed the strongest binding to Ubiquilins **(Figure S5)**. The linker between the Sti1 and FrzS domain is WSG and the linker between the FrzS domain and TMD is GNS.

Expression and Purification of Ubiquilins

Ubiquilins were expressed in BL21 DE3 cells with the pRIL plasmid (Agilent). Cells were grown in terrific broth at 37° C until OD_{600} = 0.6-0.8. Ubiquilin protein expression was induced by addition of 0.5 mM isopropyl β-D-1-thiogalactopyranoside (IPTG, RPI corp). Upon induction, temperature was dropped to 15° C and cells were incubated for 3-4 h. Cells were pelleted by centrifuging for 20' at 3900 rpm in Eppendorf 5810R centrifuge. The cell pellet from 1 L of culture was resuspended in 50 mL of UBQLN Lysis Buffer (50 mM Hepes pH 7.5, 150 mM NaCl, 1mM DTT, 0.01 mM EDTA, 10% glycerol), supplemented with 0.05 mg/mL lysozyme (Simga) and 1 mM Phenylmethylsulfonyl fluoride (PMSF). Samples were stored at -80° C until purification.

Cell pellets were thawed in water and then kept on ice throughout the procedure to minimize proteolysis. After thawing, 2 μL of Universal Nuclease (Pierce) was added to each cell pellet and volume was brought to ~120 mL by addition of lysis buffer or additional cell pellets. Cells were transferred to a metal cup surrounded by ice and lysed by sonication. The supernatant was isolated by centrifugation at 18,500 x g for 30' at 4° C and purified by Ni-NTA affinity chromatography (Thermo Fisher) on a gravity column in the cold room. Ni-NTA resin was washed with 25 column volumes (CV) of UBQLN Lysis Buffer. Sample was eluted with Lysis Buffer supplemented with 250 mM imidazole. The eluent was concentrated to < 1 mL in a 50 kDa MWCO Amicon Ultra centrifugal filter (Millipore). Sample was then incubated overnight at 4° C with a 100:1 ratio of Ubiquilin to 3C protease to remove the His_6 tag.

The protein was further purified by size exclusion chromatography (SEC) on a Superdex 200 Increase 10/300 GL, GE Healthcare in UBQLN FPLC Buffer (20 mM Tris pH 7.5, 100 mM NaCl, 1 mM DTT). Peak fractions were pooled, concentrated to 5-15 mg/mL in a 50 kDa MWCO Amicon Ultra centrifugal filter (Millipore) and aliquots were flash-frozen in liquid nitrogen and

stored at -80° C. Protein concentrations were determined by A_{280} using a calculated extinction coefficient (Expasy).

Expression and Purification of crystallization construct

The crystallization construct was grown and expressed as described above for Ubiquilins with the following changes. The crystallization construct was expressed in BL21 DE3 pRIL cells and grown in terrific broth until OD600 of 0.6-0.8, at which point expression was induced 0.5 mM IPTG at room temperature for 16 hours. Lysis Buffer is 50 mM Tris pH 7.5, 20 mM Imidazole, 500 mM NaCl, 10% glycerol, 1 mM DTT and Elution Buffer is 50 mM Tris pH 7.5, 500 mM imidazole, 150 mM NaCl, 1 mM DTT. After elution, the eluent was concentrated to < 1 mL in a 10 kDa MWCO Amicon Ultra centrifugal filter (Millipore). Sample was then mixed with a 100:1 ratio of protein to 3C protease and dialyzed overnight at 4° C in Dialysis Buffer (50 mM Tris pH 7.5, 150 mM NaCl, 1 mM β-mercaptoethanol). The protein was further purified by size exclusion chromatography (SEC) on a Superdex 200 Increase 10/300 GL column equilibrated in Dialysis Buffer. Peak fractions were pooled, concentrated to > 14 mg/mL in a 10 kDa MWCO Amicon Ultra centrifugal filter (Millipore) and aliquots were flash-frozen in liquid nitrogen and stored at -80° C. Protein concentrations were determined by A_{280} using a calculated extinction coefficient (Expasy).

Protein crystallization and structure determination

Crystals of Sti1-Frzs-TMD construct were grown at 4° C using hanging-drop vapor diffusion method by mixing equal volume (1 µL) of protein and reservoir solution containing 2.5% MPD, 100 mM Tris pH 8.5. Large crystals were grown over a period of three days and shown to belong to the space group $P12_11$. Protein crystals were then soaked 2-3 times in cryoprotectant containing the well solution and 20% glycerol and flash frozen in liquid nitrogen.
Diffraction data were collected at Beamline 8.2.2 at Advanced Light Source at Lawrence Berkeley National Laboratory (Berkeley, CA). Data were processed and scaled using Mosflm[53] and CCP4[54]. Crystals of Sti1-Frzs-TMD diffracted to 1.98 Å resolution and belong to space group $P12_11$ with unit cell dimensions a= 67.41 Å, b= 63.92 Å, and c= 67.43 Å. Phases were determined by molecular replacement using Phaser-MR[55] program incorporated in the Phenix package[56]. Receiver domain from Myxococcus xanthus social motility protein FrzS (PDB: 2GKG) was used as the search model which represents 55% of Sti1-Frzs-TMD construct. The initial solution from molecular replacement generated interpretable electron density map. Model building and refinement was carried out using COOT[57]. The resulting model was further improved by positional and anisotropic B-factor refinement in Phenix, and the model quality was monitored throughout all stages of refinement process and validated using MolProbity[58]. The atomic coordinates and structure factors are deposited in the PDB: 9CKX.

Size Exclusion Chromatography

Analytical size exclusion chromatography was performed on a BioRad NGC Quest 10 Plus with a Superdex 200 Increase 10/300 GL column (Cytiva). A total of 0.5 mL of sample at 2 mg/mL was loaded onto the column at a flow rate of 0.5 mL/min. Aldolase (158 kDa), Conalbumin (75 kDa), Ovalbumin (44 kDa), and Lysozyme (14 kDa) were used as molecular weight standards.

Barcoded Binding Assay

In Vitro Translation (IVT) was performed using the PURExpress in vitro protein synthesis kit (NEB). Each IVT reaction contained 4 µL of PURE Solution A, 3 µL of PURE Solution B, 1 µL of EasyTag L-[^{35}S] methionine stabilized aqueous solution (Perkin Elmer), 0.2 µL of Superase-in RNase inhibitor (Invitrogen), 100 ng of plasmid DNA, and a final concentration of 3 µM Ubiquilin.

Nuclease free water was added to bring the total reaction volume to 10 μL. The reaction was incubated at 37° C for 2 h.

The barcoded binding assay was performed with a mixture of each of the six plasmids such that there was roughly equal expression of each construct. The ratio of each plasmid was determined empirically by running individual IVT reactions for each plasmid within a substrate series. All six reactions were run on the same SDS PAGE gel and analyzed by autoradiography and ImageJ.

After the 2 h incubation, the IVT reaction was diluted with 40 μL of Wash Buffer (20 mM Tris pH 7.5, 100mM NaCl, 1 mg/mL BSA). A 5 μL sample was taken as the "INPUT" fraction. The remaining 45 μL were added to 2 μL of settled anti-Flag magnetic beads (4 μL of 50% slurry) (Thermo Fisher) that had been equilibrated in Wash Buffer. Sample was allowed to bind to resin for 30' at 4° C before 20 μL of sample were taken for the "FLOW THROUGH" fraction, the remaining flow through was discarded. Beads were then washed 4x with 1 mL of wash buffer at 4° C for 10'. After the final wash, 40 μL of sample were taken for the "WASH" fraction. To elute Ubiquilins, 25 μL of Wash Buffer containing 1 mg/mL 3x Flag Peptide (ApexBio) was added and the sample was incubated in the Thermomixer at 37° C for 30'. All 25 μL were taken for the "ELUTE" fraction.

The "INPUT", "FLOW THROUGH", "WASH", AND "ELUTE" fractions were brought to a final volume of 50 μL by adding MilliQ Water and then 16.6 μL of 4x SDS PAGE Loading Buffer was added to the samples. Samples were then run on a 4-20% gradient Criterion gel (Bio-Rad), stained with Coomassie, and imaged. Gel was then incubated in drying solution (40% methanol, 10% glycerol, 7.5% acetic acid) for 5'. Gel was then placed into a gel drying apparatus (Promega) and allowed to sit at room temperature for 12-16 h with a fan on the apparatus. Dried gel was then exposed to X-ray film (RPI corp) for 24 h and then developed. Band intensity was measured using ImageJ.

Software
The ImageJ software was downloaded here https://imagej.nih.gov/
GRAVY scores were calculated here https://www.gravy-calculator.de/
Agadir scores were calculated here http://agadir.crg.es/

Acknowledgements
The authors wish to thank members of the Castañeda and Wohlever labs for helpful discussions and feedback on the project.
Funding: This work was supported by NSF CAREER Award 2343131 (MLW), NIH grant R35 GM137904-01S2 (MLW). The ALS ENABLE beamlines are supported in part by the National Institutes of Health, National Institute of General Medical Sciences, grant P30 GM124169-01. The Advanced Light Source is a Department of Energy Office of Science User Facility under Contract No. DE-AC02-05CH11231.
Author Contributions: Conceptualization: JO, MLW; Methodology: JO, SB, SA; Investigation: JO, SB, SA; Crystallography Data Collection: BS; Structure determination: SB; Writing – Original Draft: JO, MLW; Writing – Review and Editing: SB, SA, MLW; Supervision and Funding Acquisition: MLW
Competing Interests: The authors declare no competing interests.

Supplemental Figures

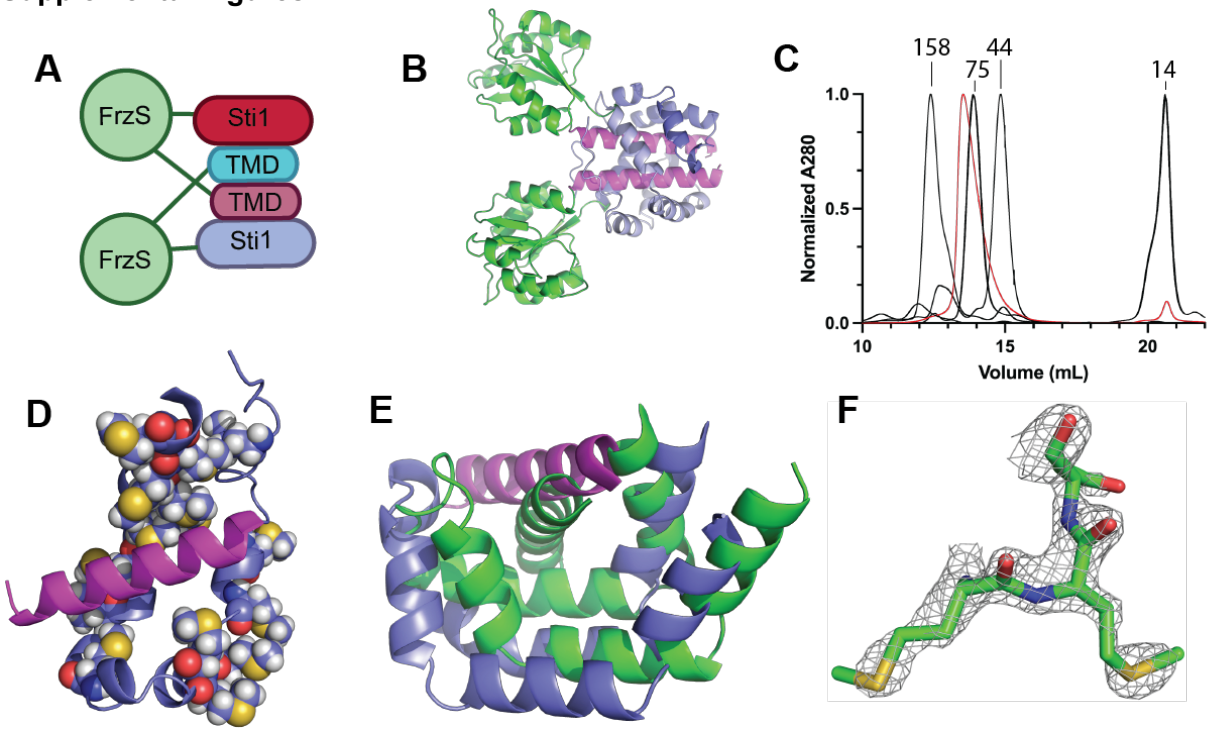

Figure S1: Crystal structure of the Dsk2 Sti1 domain bound to a TMD

A) Diagram showing the domain swap in the crystal structure.
B) The FrzS domain does not drive dimerization and has minimal contacts with the Sti1 domain.
C) Size exclusion chromatography shows that the crystallization construct (red), which has a molecular weight of 24.4 kDa, runs as an oligomer. Molecular weight of standards (Aldolase, Conalbumin, Ovalbumin, and Lysozyme) are noted on the chart.
D) The hydrophobic groove is enriched for methionine residues, which are shown as spheres.
E) Comparison of the crystal structure (slate and magenta) with the AlphaFold prediction (green). FrzS domains omitted for clarity.
F) Fitting of the final refined model for residues 68-70 in the σA-weighted 2*Fo*-*Fc* electron density map contoured at 3 sigma.

A

```
                      P189T
MB Dsk2 165 EQLEGIMLSPAFQEQMNALMLDPRMLDMMIDQNPQLRNMG  204
UBQLN2  180 EMMIQIMENPFVQ----SMLSNPDLMRQLIMANPQMQQLI  215

MB Dsk2 205 PEARQMLRPMFREMMSNPESMRSMMNMGRA   234
UBQLN2  216 Q-----RNPEISHLLNNPDIMRQTLEIARN   240
```

B

```
MB Dsk2 165 EQLEGIMLSPAFQEQMNALMLDPRMLDMMI------DQNPQLRN 202
UBQLN2  381 QLMQNMLSAPYMRSMMQSLSQNPDLAAQMMLNNPLFAGNPQLQE 432

                Q425R          P440L M446R
MB Dsk2 203 MGPEARQMLRPMFREMMSNPESMRSM---------MNMGRA-  234
UBQLN2  433 ----QMRPQLPAFLQQMQNPDTLSAMSNPRAMQALMQIQQGL  462
```

Figure S2: Sequence alignment of *M. bicuspidata* Dsk2 with UBQLN2
Sequence alignment between *M. bicuspidata* Dsk2 and the UBQLN2 Sti1-I **(A)** or Sti1-II **(B)** domain. Separate alignments for Sti1-I and Sti1-II were performed in Clustal Omega using the annotated domains from UBQLN1, UBQLN2, & UBQLN4. For clarity, only UBQLN2 is shown. This alignment was used to map UBQLN2 ALS mutations onto the Dsk2 structure for analysis in Figure 2.

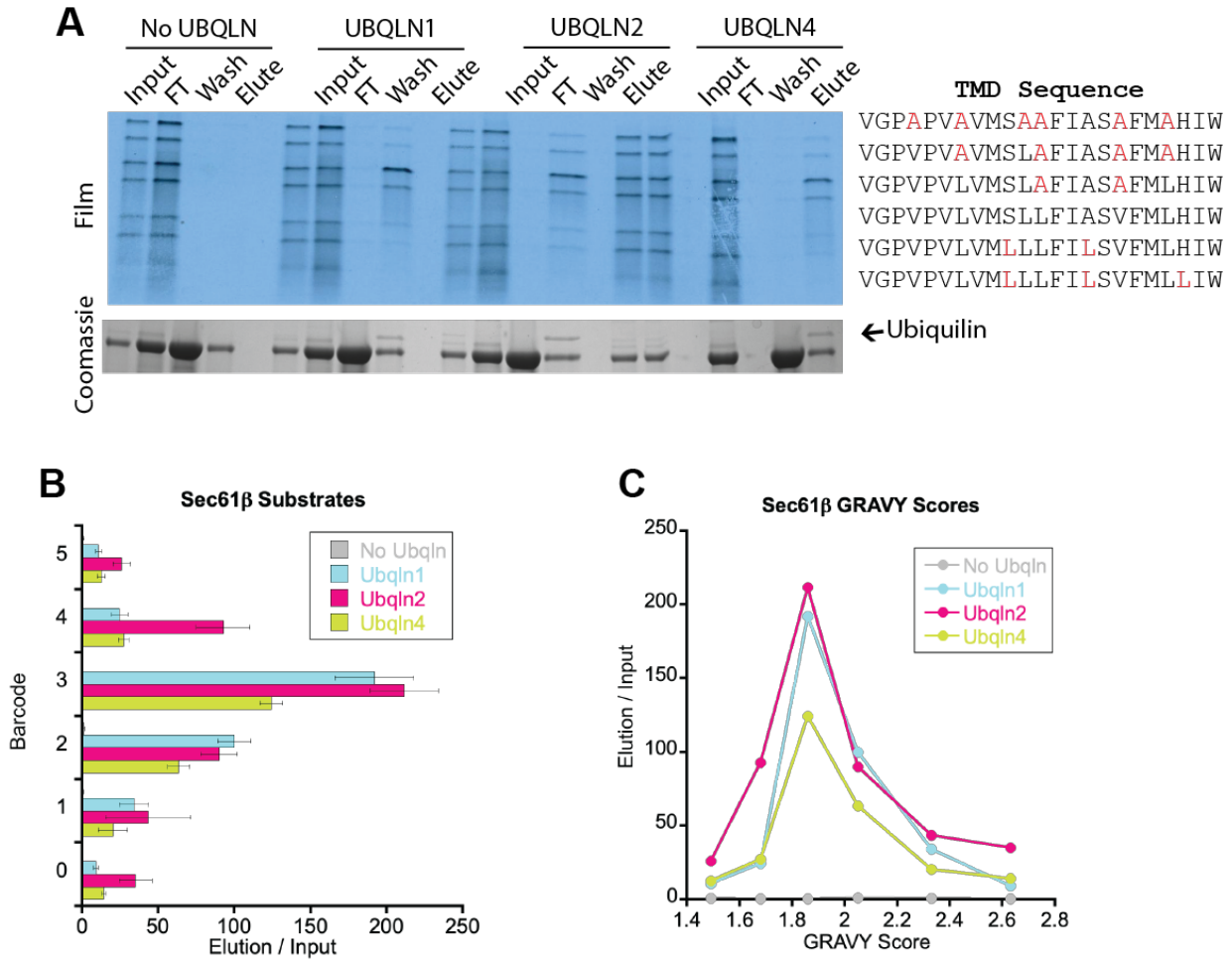

Figure S3: Barcoded binding data with the Sec61β substrate series

A) Barcoded binding assay with the Sec61β substrate series. The wild type Sec61β TMD has a barcode of 2.

B) Quantification of the data in A, organized by barcode. A value of 100 corresponds to equal intensity of input and elution bands.

C) Quantification of the data in A, organized by TMD hydrophobicity (GRAVY score). Error bars omitted for clarity.

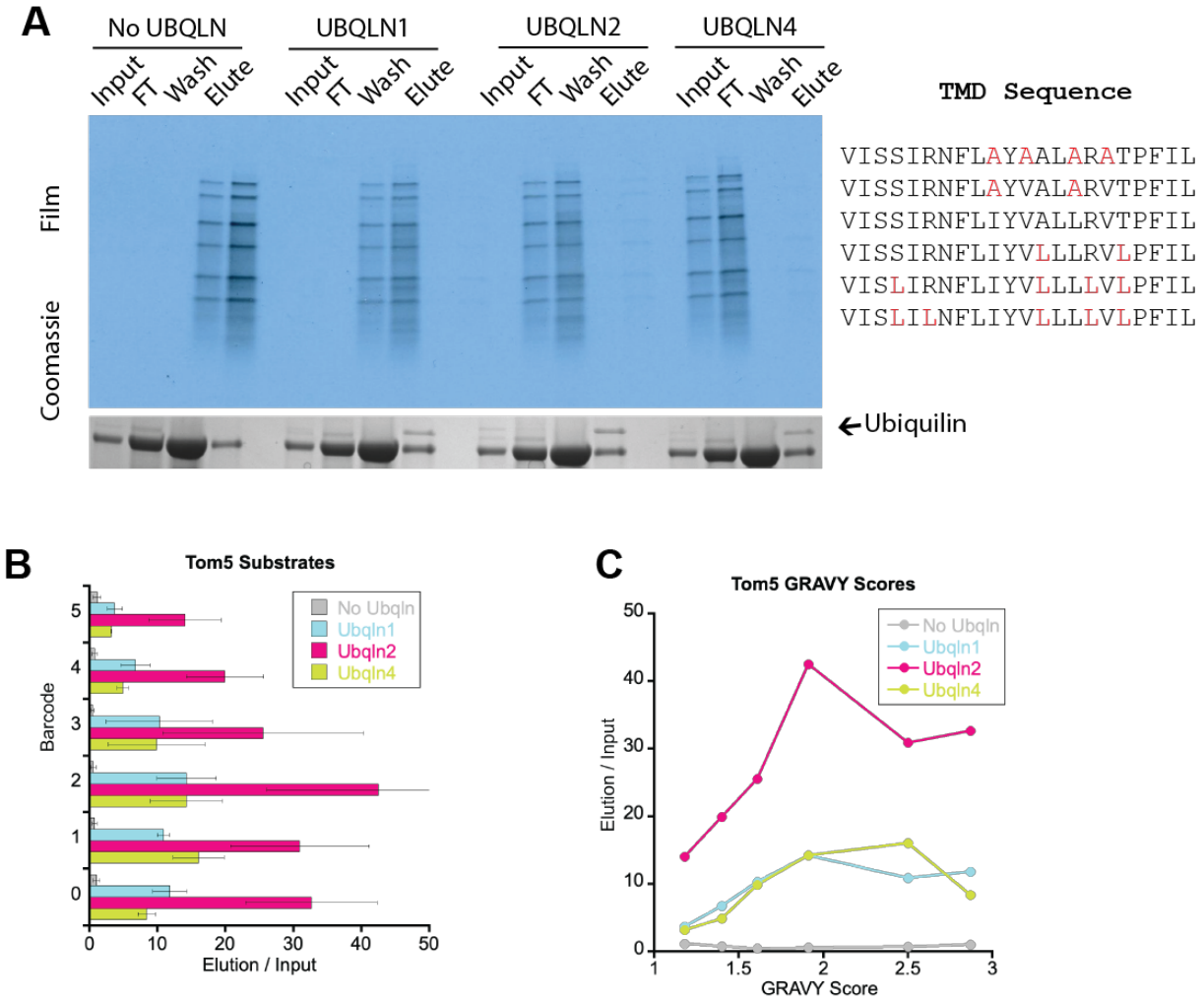

Figure S4: Barcoded binding data with the Tom5 substrate series

A) Barcoded binding assay with the Tom5 substrate series. The wild type Tom5 TMD has a barcode of 3.

B) Quantification of the data in A, organized by barcode. A value of 100 corresponds to equal intensity of input and elution bands.

C) Quantification of the data in A, organized by TMD hydrophobicity (GRAVY score). Error bars omitted for clarity.

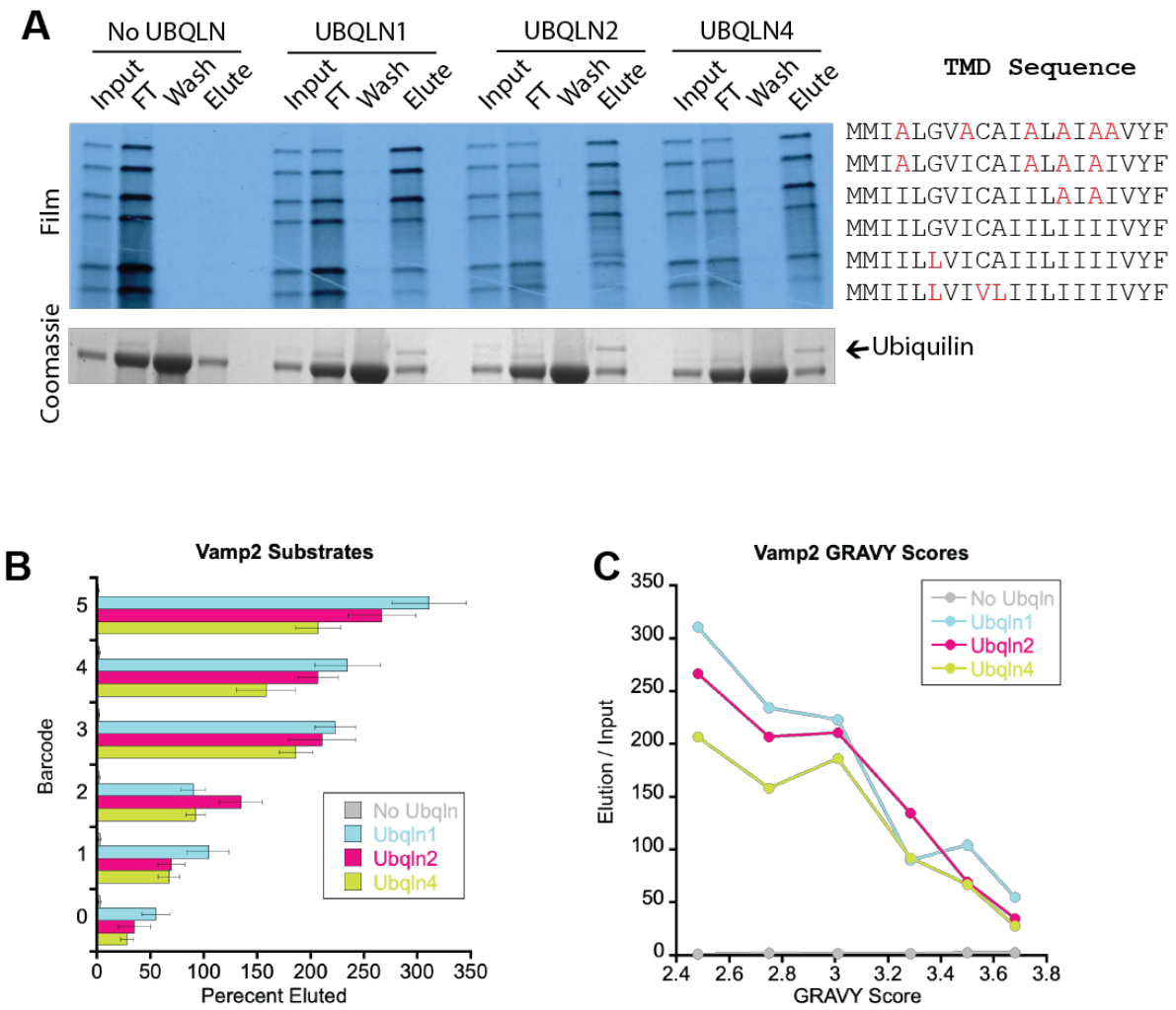

Figure S5: Barcoded binding data with the Vamp2 substrate series

A) Barcoded binding assay with the Vamp2 substrate series. The wild type Vamp2 TMD has a barcode of 2.

B) Quantification of the data in A, organized by barcode. A value of 100 corresponds to equal intensity of input and elution bands.

C) Quantification of the data in A, organized by TMD hydrophobicity (GRAVY score). Error bars omitted for clarity.

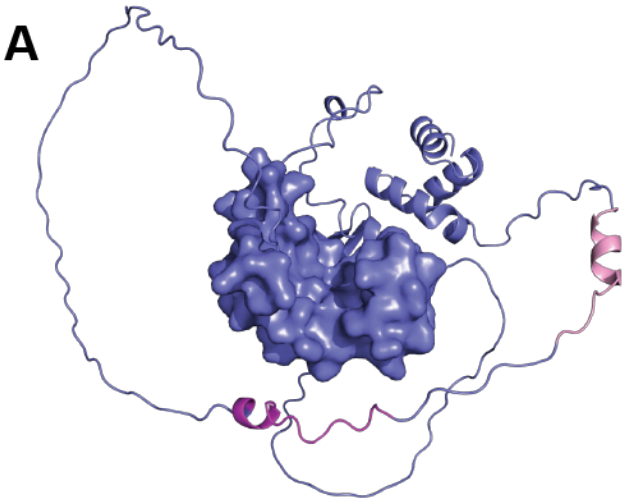

B

Residues	Sequence	GRAVY	Agadir
279-291	FASLLNPALNPFA	0.88	0.03
302-313	MPAFDPALLASMF	1.15	1.85

Figure S6: Putative helices in AlphaFold model of Dsk2

A) AlphaFold model of *S. cerevisiae* Dsk2 highlighting short, putative helices within otherwise disordered sequences. Sti1 domain is shown as a surface.
B) The putative helices identified in A have GRAVY and Agadir scores that would allow for suboptimal binding to the Sti1 domain as is expected for a placeholder sequence that also serves as a selectivity filter.

References

1. Lee, D. Y. & Brown, E. J. Ubiquilins in the crosstalk among proteolytic pathways. *Biological chemistry* **393**, 441–447 (2012).

2. Zheng, T., Yang, Y. & Castañeda, C. A. Structure, dynamics and functions of UBQLNs: at the crossroads of protein quality control machinery. *Biochem J* **477**, 3471–3497 (2020).

3. Ma, Q. *et al.* UBQLN2 and HSP70 participate in Parkin-mediated mitophagy by facilitating outer mitochondrial membrane rupture. *EMBO Rep.* e55859 (2023) doi:10.15252/embr.202255859.

4. Black, H. H. *et al.* UBQLN2 restrains the domesticated retrotransposon PEG10 to maintain neuronal health in ALS. *Elife* **12**, e79452 (2023).

5. Whiteley, A. M. *et al.* Ubiquilin1 promotes antigen-receptor mediated proliferation by eliminating mislocalized mitochondrial proteins. *eLife* **6**, 403 (2017).

6. Lin, B. C., Higgins, N. R., Phung, T. H. & Monteiro, M. J. UBQLN proteins in health and disease with a focus on UBQLN2 in ALS/FTD. *Febs J* (2021) doi:10.1111/febs.16129.

7. Alexander, E. J. *et al.* Ubiquilin 2 modulates ALS/FTD-linked FUS–RNA complex dynamics and stress granule formation. *Proceedings of the National Academy of Sciences* **5**, 201811997 (2018).

8. Riley, J. F., Fioramonti, P. J., Rusnock, A. K., Hehnly, H. & Castañeda, C. A. ALS-linked mutations impair UBQLN2 stress-induced biomolecular condensate assembly in cells. *J Neurochem* (2021) doi:10.1111/jnc.15453.

9. Deng, H.-X. *et al.* Mutations in UBQLN2 cause dominant X-linked juvenile and adult-onset ALS and ALS/dementia. *Nature* **477**, 211–215 (2011).

10. Edens, B. M. *et al.* A novel ALS-associated variant in UBQLN4 regulates motor axon morphogenesis. *eLife* **6**, e25453 (2017).

11. Fahed, A. C. *et al.* UBQLN2 Mutation Causing Heterogeneous X-linked Dominant Neurodegeneration. *Annals of neurology* (2014) doi:10.1002/ana.24164.

12. Bertram, L. *et al.* Family-based association between Alzheimer's disease and variants in UBQLN1. *New England Journal of Medicine* **352**, 884–894 (2005).

13. Douglas, P. M. & Dillin, A. Protein homeostasis and aging in neurodegeneration. *J. Cell Biol.* **190**, 719–729 (2010).

14. Safren, N. *et al.* Pathogenic mutations in UBQLN2 exhibit diverse aggregation propensity and neurotoxicity. *Sci. Rep.* **14**, 6049 (2024).

15. Hjerpe, R. *et al.* UBQLN2 Mediates Autophagy-Independent Protein Aggregate Clearance by the Proteasome. *Cell* **166**, 935–949 (2016).

16. Kleijnen, M. F. *et al.* The hPLIC proteins may provide a link between the ubiquitination machinery and the proteasome. *Molecular Cell* **6**, 409–419 (2000).

17. Walters, K. J., Kleijnen, M. F., Goh, A. M., Wagner, G. & Howley, P. M. Structural studies of the interaction between ubiquitin family proteins and proteasome subunit S5a. *Biochemistry* **41**, 1767–1777 (2002).

18. Dantuma, N. P., Heinen, C. & Hoogstraten, D. The ubiquitin receptor Rad23: At the crossroads of nucleotide excision repair and proteasomal degradation. *DNA Repair* **8**, 449–460 (2009).

19. Stieren, E. S. *et al.* Ubiquilin-1 Is a Molecular Chaperone for the Amyloid Precursor Protein. *Journal of Biological Chemistry* **286**, 35689–35698 (2011).

20. Kurlawala, Z., Shah, P. P., Shah, C. & Beverly, L. J. The STI and UBA Domains of UBQLN1 are Critical Determinants of Substrate Interaction and Proteostasis. *Journal of Cellular Biochemistry* 1–27 (2017) doi:10.1002/jcb.25880.

21. Itakura, E. *et al.* Ubiquilins Chaperone and Triage Mitochondrial Membrane Proteins for Degradation. *Molecular Cell* **63**, (2016).

22. Rao, M. *et al.* Multiple selection filters ensure accurate tail-anchored membrane protein targeting. *eLife* (2016) doi:10.7554/elife.21301.001.

23. Guna, A. & Hegde, R. S. Transmembrane Domain Recognition during Membrane Protein Biogenesis and Quality Control. *Current Biology* **28**, R498–R511 (2018).

24. Pleiner, T. *et al.* A selectivity filter in the ER membrane protein complex limits protein misinsertion at the ER. *J Cell Biol* **222**, e202212007 (2023).

25. Stefer, S. *et al.* Structural basis for tail-anchored membrane protein biogenesis by the Get3-receptor complex. *Science (New York, NY)* **333**, 758–762 (2011).

26. Fry, M. Y., Saladi, S. M. & Clemons, W. M. The STI1-domain is a flexible alpha-helical fold with a hydrophobic groove. *Protein Sci* **30**, 882–898 (2021).

27. Lin, K.-F., Fry, M. Y., Saladi, S. M. & Clemons, W. M. Molecular basis of tail-anchored integral membrane protein recognition by the cochaperone Sgt2. *J Biol Chem* 100441 (2021) doi:10.1016/j.jbc.2021.100441.

28. Jumper, J. *et al.* Highly accurate protein structure prediction with AlphaFold. *Nature* **596**, 583–589 (2021).

29. Dao, T. P. *et al.* Ubiquitin Modulates Liquid-Liquid Phase Separation of UBQLN2 via Disruption of Multivalent Interactions. *Molecular Cell* **69**, 965-978.e6 (2018).

30. Dao, T. P. & Castañeda, C. A. Ubiquitin-Modulated Phase Separation of Shuttle Proteins: Does Condensate Formation Promote Protein Degradation? *Bioessays* **42**, 2000036 (2020).

31. Dao, T. P. *et al.* Mechanistic insights into enhancement or inhibition of phase separation by different polyubiquitin chains. *Embo Rep* **23**, e55056 (2022).

32. Fraser, J. S. *et al.* An atypical receiver domain controls the dynamic polar localization of the Myxococcus xanthus social motility protein FrzS. *Mol. Microbiol.* **65**, 319–332 (2007).

33. Maurer, S. K. *et al.* Ubiquitin-specific protease 11 structure in complex with an engineered substrate mimetic reveals a molecular feature for deubiquitination selectivity. *J. Biol. Chem.* **299**, 105300 (2023).

34. Mateja, A. *et al.* Protein targeting. Structure of the Get3 targeting factor in complex with its membrane protein cargo. *Science (New York, NY)* **347**, 1152–1155 (2015).

35. Ford, D. L. & Monteiro, M. J. Dimerization of ubiquilin is dependent upon the central region of the protein: evidence that the monomer, but not the dimer, is involved in binding presenilins. *The Biochemical journal* **399**, 397 (2006).

36. Zheng, T., Galagedera, S. K. K. & Castañeda, C. A. Previously uncharacterized interactions between the folded and intrinsically disordered domains impart asymmetric effects on UBQLN2 phase separation. *Protein Sci* **30**, 1467–1481 (2021).

37. Hegde, R. S. & Keenan, R. J. The mechanisms of integral membrane protein biogenesis. *Nat Rev Mol Cell Bio* **23**, 107–124 (2022).

38. Richardson, J. S. & Richardson, D. C. Amino Acid Preferences for Specific Locations at the Ends of α Helices. *Science* **240**, 1648–1652 (1988).

39. Shimizu, Y. *et al.* Cell-free translation reconstituted with purified components. *Nature Biotechnology* **19**, 751–755 (2001).

40. Guna, A. *et al.* MTCH2 is a mitochondrial outer membrane protein insertase. *Science* **378**, 317–322 (2022).

41. Kyte, J. & Doolittle, R. F. A simple method for displaying the hydropathic character of a protein. *J. Mol. Biol.* **157**, 105–132 (1982).

42. Kurochkina, N. & Guha, U. SH3 domains: modules of protein–protein interactions. *Biophys. Rev.* **5**, 29–39 (2013).

43. Muñoz, V. & Serrano, L. Elucidating the folding problem of helical peptides using empirical parameters. *Nat Struct Biol* **1**, 399–409 (1994).

44. Muñoz, V. & Serrano, L. Elucidating the Folding Problem of Helical Peptides using Empirical Parameters. III>Temperature and pH Dependence. *J Mol Biol* **245**, 297–308 (1995).

45. Muñoz, V. & Serrano, L. Elucidating the Folding Problem of Helical Peptides using Empirical Parameters. III>Temperature and pH Dependence. *J Mol Biol* **245**, 297–308 (1995).

46. Rao, M. *et al.* Multiple selection filters ensure accurate tail-anchored membrane protein targeting. *eLife* **5**, e21301 (2016).

47. Wang, S.-H., Zheng, T. & Fawzi, N. L. Structure and interactions of prion-like domains in transcription factor Efg1 phase separation. *Biophys. J.* **123**, 1481–1493 (2024).

48. Conicella, A. E., Zerze, G. H., Mittal, J. & Fawzi, N. L. ALS Mutations Disrupt Phase Separation Mediated by α-Helical Structure in the TDP-43 Low-Complexity C-Terminal Domain. *Structure* **24**, 1537–1549 (2016).

49. Buel, G. R. *et al.* E6AP AZUL interaction with UBQLN1/2 in cells, condensates, and an AlphaFold-NMR integrated structure. *Structure* **31**, 395-410.e6 (2023).

50. Dao, T. P., Rajendran, A., Galagedera, S. K. K., Haws, W. & Castañeda, C. A. Short disordered termini and proline-rich domain are major regulators of UBQLN1/2/4 phase separation. *Biophys. J.* **123**, 1449–1457 (2024).

51. Voorhees, R. M. & Hegde, R. S. Structure of the Sec61 channel opened by a signal sequence. *Science (New York, NY)* **351**, 88–91 (2016).

52. Dao, T. P. *et al.* ALS-Linked Mutations Affect UBQLN2 Oligomerization and Phase Separation in a Position- and Amino Acid-Dependent Manner. *Structure* **27**, 937-951.e5 (2019).

53. Battye, T. G. G., Kontogiannis, L., Johnson, O., Powell, H. R. & Leslie, A. G. W. iMOSFLM: a new graphical interface for diffraction-image processing with MOSFLM. *Acta Crystallogr. Sect. D: Biol. Crystallogr.* **67**, 271–281 (2011).

54. Agirre, J. *et al.* The CCP4 suite: integrative software for macromolecular crystallography. *Acta Crystallogr. Sect. D* **79**, 449–461 (2023).

55. McCoy, A. J. *et al.* Phaser crystallographic software. *Journal of applied crystallography* **40**, 658–674 (2007).

56. Adams, P. D. *et al.* PHENIX: a comprehensive Python-based system for macromolecular structure solution. *Acta Crystallogr. Sect. D: Biol. Crystallogr.* **66**, 213–221 (2010).

57. Emsley, P., Lohkamp, B., Scott, W. G. & Cowtan, K. Features and development of Coot. *Acta crystallographica. Section D, Biological crystallography* **66**, 486–501 (2010).

58. Williams, C. J. *et al.* MolProbity: More and better reference data for improved all-atom structure validation. *Protein Sci.* **27**, 293–315 (2018).